Title
In vivo local determination of tissue optical properties: applications to human brain.

Journal
Applied Optics, 38(22)

ISSN
0003-6935

Authors
Bevilacqua, F
Piguet, D
Marquet, P
et al.

Publication Date
1999-08-01

DOI
10.1364/ao.38.004939

In vivo local determination of tissue optical properties: applications to human brain

Frédéric Bevilacqua, Dominique Piguet, Pierre Marquet, Jeffrey D. Gross, Bruce J. Tromberg, and Christian Depeursinge

Local and superficial near-infrared (NIR) optical-property characterization of turbid biological tissues can be achieved by measurement of spatially resolved diffuse reflectance at small source–detector separations (<1.4 mm). However, in these conditions the inverse problem, i.e., calculation of localized absorption and the reduced scattering coefficients, is necessarily sensitive to the scattering phase function. This effect can be minimized if a new parameter of the phase function γ, which depends on the first and the second moments of the phase function, is known. If γ is unknown, an estimation of this parameter can be obtained by the measurement, but the uncertainty of the absorption coefficient is increased. A spatially resolved reflectance probe employing multiple detector fibers (0.3–1.4 mm from the source) is described. Monte Carlo simulations are used to determine γ, the reduced scattering and absorption coefficients from reflectance data. Probe performance is assessed by measurements on phantoms, the optical properties of which were measured by other techniques [frequency domain photon migration (FDPM) and spatially resolved transmittance]. Our results show that changes in the absorption coefficient, the reduced scattering coefficient, and γ can be measured to within $\pm 0.005\ \mathrm{mm}^{-1}$, $\pm 0.05\ \mathrm{mm}^{-1}$, and ± 0.2, respectively. *In vivo* measurements performed intraoperatively on a human skull and brain are reported for four NIR wavelengths (674, 811, 849, 956 nm) when the spatially resolved probe and FDPM are used. The spatially resolved probe shows optimum measurement sensitivity in the measurement volume immediately beneath the probe (typically 1 mm^3 in tissues), whereas FDPM typically samples larger regions of tissues. Optical-property values for human skull, white matter, scar tissue, optic nerve, and tumors are reported that show distinct absorption and scattering differences between structures and a dependence on the phase-function parameter γ.

OCIS codes: 170.7050, 290.4210, 170.3660, 170.5280, 170.4550, 170.6510.

1. Introduction

Probing the optical properties of biological tissues has a major effect in several medical applications for diagnosis and therapy. For example, the knowledge of these properties is necessary for optimizing techniques such as near-IR spectroscopy or photodynamic therapy. The scattering and the absorption characteristics of many different kinds of tissues have been reported in the literature.[1] However, they have been most often measured *in vitro*. Because of unavoidable alterations in excised samples, such as blood drainage, structural alterations, and temperature changes, these values are questionable and *in vivo* measurements are preferred.

Measurement of optical properties performed *in vivo* could also be used as a diagnostic tool, which is complementary to other optical biopsy techniques, e.g., tissue autofluorescence. Indeed light scattering and absorption can provide information both on tissue structure and on chromophore content, features that can be used to distinguish between normal tissues, malignant lesions, and other pathologies. For example, hemoglobin and water content have been found to be significantly different in normal and cancerous tissues.[2,3] Differentiation between normal and malignant bladder tissues[4] was found to be possible from the elastic scattering and absorption properties.

F. Bevilacqua, D. Piguet, P. Marquet, and C. Depeursinge (christian.depeursinge@epfl.ch) are with the Department of Micro-Engineering, Institute of Applied Optics, Swiss Federal Institute of Technology Lausanne, 1015 Lausanne, Switzerland. J. D. Gross and B. J. Tromberg are with the Laser Microbeam and Medical Program, Beckman Laser Institute and Medical Clinic, University of California, Irvine, 1002 Health Sciences Road East, Irvine, California 92612. J. D. Gross is also with the Division of Neurological Surgery, University of New Mexico School of Medicine, Albuquerque, New Mexico 87131.

Received 4 January 1999; revised manuscript received 5 May 1999.

0003-6935/99/224939-12$15.00/0

Researchers have proposed different methods to determine quantitatively absorption and reduced scattering coefficients *in vivo*, by using spatially[5–7] and/or temporally resolved measurements.[2,3,8,9] Besides organs such as breast or neonatal brain, which can be transilluminated, measurements of thick tissues can be made in reflectance geometry. The case in which source–detector separations are larger than several transport mean-free paths, corresponding typically to distances greater than 5 mm for biological tissues, has been extensively studied theoretically and experimentally. Diffusion theory or Monte Carlo simulations have been commonly used to relate the measured light intensity to the optical coefficients. In particular, optimized source–detector separations have been calculated by different authors[6,10] to ensure the best sensitivity to absorption and scattering coefficients from spatially resolved reflectance data. For typical turbid tissues, the optimal determination of both absorption and scattering properties requires reflectance measurement at small and large distances. For example, measurements were performed by Farrell *et al*.[5] using distances from 1 to 10 mm and by Bays *et al*.[6] using distances from 3.6 to 15 mm or 2 to 14 mm.

Nevertheless in all these studies the turbid medium is considered homogeneous or made of homogeneous layers. Our approach is different. We wish to characterize optically a small volume of tissue, of the order of a few cubic millimeters, possibly distinct from surrounding tissues. Therefore our goal is to differentiate a small tissue heterogeneity instead of determining average optical properties of a large volume of tissue. To achieve this, we chose to perform spatially resolved reflectance measurements with only small source–detector separations, from 0.3 to 1.4 mm, even if these distances are not optimal for absorption determination.

Mourant *et al*.[4,11] have shown that the absorption coefficient can be estimated from measurement at a single distance of ~1.7 mm, assuming the scattering coefficient to be in a certain range. They have also shown that measurements at a single shorter distance (~0.2–0.3 mm) allows monitoring of spectroscopic variations in the scattering properties of tissues. In this research we address a general case in which both tissue scattering and absorption properties are simultaneously estimated from measurements at distances smaller than 1.4 mm.

The theoretical framework for interpretation of the measured profile in terms of absorption and scattering properties[12,13] was given in a previous study based on Monte Carlo simulations. The role of the phase function at short source–detector separations was carefully studied. In particular, we showed that, besides absorption and reduced scattering coefficients, a parameter depending on the first and the second moment of the phase function must be taken into account for source–detector separation ranging approximately from 0.3 to 10 transport mean free paths. This analysis is more complete compared with previous research in which only the first moment of the phase function (the anisotropy factor) was considered.

First we describe the probe design and the Monte Carlo model developed to simulate the measured profile. Second we discuss the average tissue volume probed and sensitivity to medium boundaries from experiments and simulations. Third we describe how the scattering and the absorption properties of tissues can be deduced from reflectance data. The accuracy of the proposed procedure is demonstrated on phantoms, the optical properties of which are measured by others techniques. Finally we present and discuss measurements of human brain obtained *in vivo*. These clinical measurements were performed in parallel with a complementary method, frequency domain photon migration (FDPM),[2,3] which probes a larger tissue volume. Optical properties from FDPM measurements are compared with values that we obtained by the spatially resolved method described here, using small source–detector separations.

2. Materials and Methods

A. Definitions

The spatially resolved reflectance is denoted $R(\rho)$, where ρ is the source–detector separation. It is defined by the backscattered power received by a detector per unit area for a source of power unity. In our measurements ρ ranges between 0.3 and 1.4 mm.

The optical properties of tissues are the average refractive index n of the medium, the absorption coefficient μ_a, the scattering coefficient μ_s, and the phase function $p(\cos\theta)$, where θ is the scattering angle. The phase function is the probability density function for $\cos\theta$. We consider the refractive index of tissues[14] as a constant, $n = 1.4$.

It is also useful to define the reduced scattering coefficient $\mu_s' = \mu_s(1 - g)$ and the transport mean free path, $mfp' = (\mu_s' + \mu_a)^{-1}$, where g is the anisotropy factor and is defined as the average of $\cos\theta$. Generally the reduced scattering coefficient μ_s' and the absorption coefficient μ_a are used to characterize optically thick tissue. Indeed for a high albedo medium the light fluence rate depends only on μ_s' and μ_a at distances of several transport mean free paths (typically $\rho > 5$ mm for tissues) from the source (diffusion approximation). Therefore use of μ_s' and μ_a is a natural choice if measurements are performed at such distances. Because we want to take measurements at closer distances, in the range of one transport mean free path we expect that some parameters of the phase function must be taken into account. This theoretical problem was fully studied with Monte Carlo simulations and reported in Refs. 12 and 13. We consider below only the main implications of this research.

For distances between 0.3 and 10 transport mean free paths we found that the reflectance curve depends on μ_a, μ_s', and a third parameter $\gamma = (1 - g_2)/(1 - g_1)$, where g_1 and g_2 are, respectively, the

first and the second moments of the phase function. The n^{th} moment g_n is defined as:[15,16]

$$g_n = \int_{-1}^{1} P_n(\cos\theta)p(\cos\theta)d(\cos\theta), \qquad (1)$$

where P_n is the Legendre polynomial of order n. Note that the first moment g_1 is the anisotropy factor g. The parameter γ is derived from the second-order similarity relations derived by Wyman *et al.*,[15] which are valid for a second-order anisotropic radiance (i.e., the radiance can be expanded as a series of Legendre polynomials of the order of at most 2). For comparison, note that the diffusion approximation and first-order similarity relation correspond to a first-order anisotropic radiance (i.e., the radiance can be expanded as a series of Legendre polynomials of the order of at most 1). The role of the parameter, $\gamma = (1 - g_2)/(1 - g_1)$, implies that the anisotropy factor g $(=g_1)$ alone is not sufficient to predict correctly the reflectance curve close to the source.

From this analysis, each tissue can be potentially characterized by three parameters: μ_a, μ_s', and γ. However, owing to the restricted range of the source–detector distances that we want to use, the simultaneous determination of μ_a, μ_s', and γ is not always possible with a high degree of accuracy. The achievable accuracy depends on the optical properties themselves and on experimental uncertainties. This problem is addressed in Section 3 for both phantom and tissue measurements.

The parameter γ may give interesting information about the tissue structure. Indeed, as measured by several authors,[17–20] the tissue phase function can be approximated by summing a highly anisotropic phase function, $p_{HA}(\cos\theta)$, due to large particles, plus a low anisotropic phase function, $p_{LA}(\cos\theta)$, due to small particles:

$$p_{\text{tissue}}(\cos\theta) = (1 - \alpha)p_{HA}(\cos\theta) + \alpha p_{LA}(\cos\theta). \qquad (2)$$

The coefficient α is introduced to guarantee the normalization of $p_{\text{tissue}}(\cos\theta)$.

The first term $p_{HA}(\cos\theta)$ has been fitted to the Rayleigh–Gans phase function[21] or to the Henyey–Greenstein phase function,[17,18] $p_{\text{HG}}(\cos\theta)$:

$$p_{\text{HG}}(\cos\theta) = \frac{1 - {g_{\text{HG}}}^2}{2(1 + {g_{\text{HG}}}^2 - 2g_{\text{HG}}\cos\theta)^{3/2}}. \qquad (3)$$

The moments of the Henyey–Greenstein phase function are given by $g_n = {g_{\text{HG}}}^n$ $(n > 0)$.

The second term, $p_{\text{LA}}(\cos\theta)$, can be interpreted as a Rayleigh-scattering contribution, valid for small scatterers compared with the wavelength. It has been approached by a purely isotropic term[17,21] or a Henyey–Greenstein phase function with a low negative g value.[18] We propose using the Rayleigh phase function[16]:

$$p_{\text{Rayleigh}}(\cos\theta) = \frac{3}{8}(1 + \cos^2\theta). \qquad (4)$$

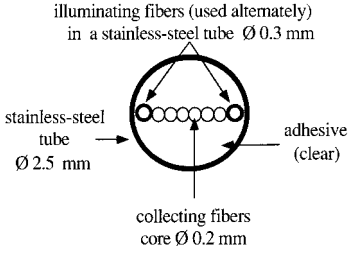

Fig. 1. Probe for measuring spatially resolved reflectance.

The moments of the Rayleigh phase function are $g_1 = 0$, $g_2 = 0.1$, $g_3 = 0$, ...

Rayleigh scattering contributes nothing to the first moment g_1 but only to the second moment g_2. The moments of the tissue phase function $p_{\text{tissue}}(\cos\theta)$ given by Eq. (2) are therefore

$$g_1 = (1 - \alpha)g_{\text{HG}}, \qquad g_2 = (1 - \alpha){g_{\text{HG}}}^2 + 0.1\alpha. \qquad (5)$$

Therefore we see that parameter γ is influenced by the relative concentration of Rayleigh scatterer α, which should depend on tissue structure.

Published phase-function data suggest possible values of γ for biological tissues.[17–20] These phase functions have been measured in goniometric experiments on thin samples. Many artifacts can affect these measurements, such as tissue preparation and tissue thickness, and these results should be used with caution. The phase function reported by Jacques *et al.*[17] for human dermis at 633 nm leads to $\gamma = 1.4$. The phase functions of white and gray matter at $\lambda = 750$ nm measured by van der Zee *et al.*[19] give values of ~1.5. Therefore we performed p_{MHG} simulations with $\gamma = 1.5$ as a starting point. As will be discussed, fitting our experimental data to simulations performed with different values of γ estimation permits a reasonable parameter estimation.

B. Experimental Setup

The probe used for measuring the spatially resolved reflectance is described in Fig. 1. It is a linear array of optical fibers (core diameter, 200 μm; N.A. = 0.37 in air). Two source fibers can be used to illuminate the tissue. They are disposed symmetrically with regard to the collecting fibers. If the sample is homogeneous, the reflectance curve is identical with either illuminating fiber. Therefore comparing the two curves tests the heterogeneity of the investigated tissue region or detects obstructions beneath the illuminating fibers. If the two curves are close (typically with differences of less than 10%), the measurement is validated and the average of the two curves is calculated.

The illuminating fibers are slid into small stainless-steel tubes to avoid direct light coupling with the collecting fibers. The coupling between each collecting fiber has been experimentally measured and found to be less than 2%. The fiber array is set in a stainless-steel tube 2.5 mm in diameter and 20 cm long. The tube is filled with an optically clear adhesive (black adhesive may also be used). The

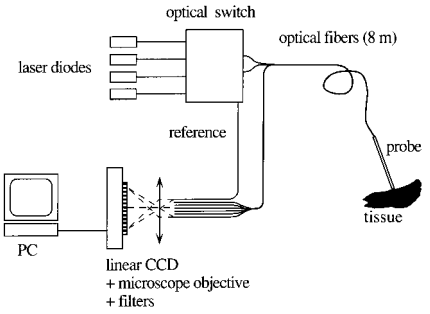

Fig. 2. Experimental setup.

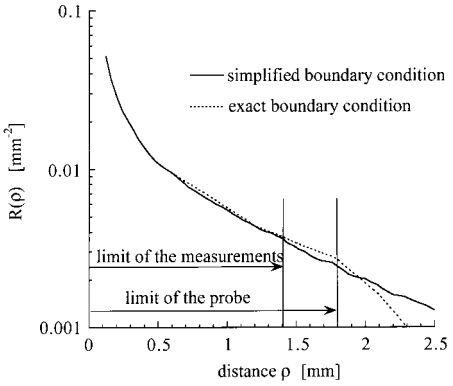

Fig. 3. Comparison between the exact and the simplified boundary conditions. The optical coefficients are $\mu_s' = 1\ \text{mm}^{-1}$, $\mu_a = 0.01\ \text{mm}^{-1}$, and $\gamma = 1.9$.

probe is rigid, which allows for easier handling by the physician, during surgery, for example. The whole probe can be sterilized. The experimental setup is shown in Fig. 2. An optical switch (Dicon Model GP700) is used to select the illuminating fiber from different sources. For the brain measurements, four laser diodes emitting at 674, 811, 849, and 956 nm were used (SDL, Inc. Models 7421, 5420, 5421, and 6321, respectively). Two other laser diodes were used for phantom measurements, emitting at 675 and 828 nm (ILEE LDA 2011 and 1805, respectively). The six fibers that collect the backscattered light are imaged on a linear CCD (Hamamatsu S3921). The signal is digitized by a 12-bit analog-to-digital card. Only one measurement, which takes ~0.1 s, is then needed to measure simultaneously the intensity collected by the six fibers. The entire system is controlled by a personal computer.

Transmission differences between each fiber are corrected by using a measurement on a turbid phantom illuminated uniformly. Immediately after each reflectance measurement, the background light is automatically measured and then subtracted from the reflectance signal. To minimize the background light, a long-pass filter ($\lambda > 650$ nm) is placed between the end of the bundle and the CCD. Even during open surgery where ambient light is substantial, the measured background ranged between 1% and 10% at the farthest fibers, depending on the wavelength used.

C. Monte Carlo Simulations

A model of photon migration in tissues is necessary to define the relationship between the measured reflectance and the optical properties. Analytical solutions from the diffusion equation are not appropriate in our case because we are interested in the reflectance close to the source, at a distance comparable with the transport mean free path (mfp′).[5,7] We performed Monte Carlo simulations to predict the measured reflectance of an homogeneous semi-infinite turbid media. The code that we used was extensively tested.[12,22,23] Any phase function can be implemented in discretized form.

Our simulations take into account the exact diameter of the illuminating and the collecting fibers as well as their numerical apertures (N.A. = 0.26 in tissue). However, the distortion of the signal due to the size of the fibers that we used ($\varnothing = 200$ nm) has an almost negligible influence on the reflectance curve.

The mismatch of the index of refraction at the surface of the medium is also taken into account in our simulation by using the Fresnel law for each photon reaching the surface. Some simulations have been performed with the exact geometry of the probe as described in Fig. 1, taking into account the mismatch of the index of refraction between the probe adhesive ($n = 1.5$) and the sample as well as the mismatch of the index of refraction between the air and the sample outside the probe ($\rho > 1.8$ mm). Photons refracted inside the lumen of the stainless-steel tube are considered absorbed. In Fig. 3 the reflectance obtained with the exact probe configuration is compared with the simplified case of the semi-infinite space ($n_{\text{medium}} = 1.4$, $n_{\text{probe}} = 1.5$). The exact-probe-boundary condition is extrapolated beyond the surface of the probe to where the boundary is tissue/air. As expected, there are important differences between the exact and the simplified cases for $\rho > 1.5$ mm, close to the limit of the probe. The decreased reflectance at $\rho > 1.8$ for the exact case is due to the increase in internal reflection at the interface between the medium and the air. However, the differences between the exact and the simplified cases are less than a few percent for $\rho < 1.4$ mm, corresponding to the region where the measurements are performed.

The simplified case, assuming cylindrical symmetry, is computationally much less time-consuming than the exact configuration. Exact-configuration simulations require ~10 times the number of photons for statistical errors to be achieved comparable for the simplified case. Indeed in the simplified case the cylindrical symmetry allows for the use of annular detectors to compute the reflectance. The advantage of annular detectors is their larger area, compared with the detector area used in the configuration of the exact-boundary condition configuration. Following the result illustrated in Fig. 3, we decided to employ only the simplified semi-infinite condition and be restricted to $\rho < 1.4$ mm.

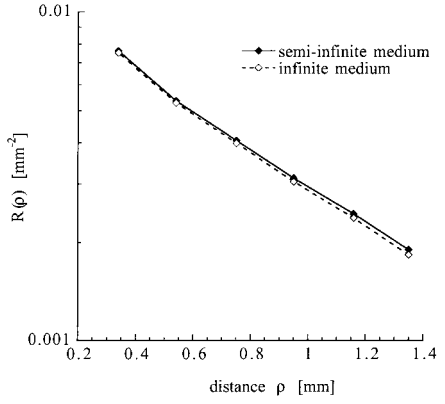

Fig. 4. Comparison between measurements in semi-infinite and in infinite media. The medium is Intralipid. The optical coefficients were measured by the FDPM technique: $\mu_s' = 1.2\ \text{mm}^{-1}$, $\mu_a = 0.0005\ \text{mm}^{-1}$ ($\lambda = 675$ nm).

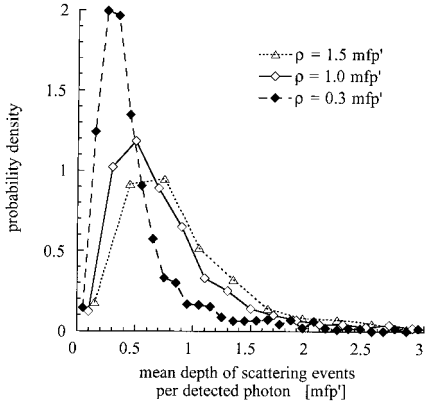

Fig. 5. Probability density of the mean depth of scattering events per detected photon for the case of $\gamma = 1.9$.

3. Results and Discussion

A. Boundary Effects

During *in vivo* investigations the ideal case of a medium with a perfect plane surface is never realized. Moreover the probe could be slightly pushed inside the tissue. Therefore the effect of the medium boundary on the measured reflectance is important to quantify experimentally. In Fig. 4 we show two measurements in Intralipid ($\lambda = 675$ nm), one at the surface and the second inside the medium. The difference between these two measurements is less than 5%, which could seem very surprising at first glance. However, as shown by simulation in Fig. 3, the boundary condition outside the probe has only a weak effect on the intensity measured by the six fibers. The boundary condition created by the probe itself, i.e., the index of refraction mismatch between the medium and the adhesive inside the probe, is much more critical.

The negligible effect of the tissue boundaries shown in this section is an important advantage for clinical investigation. This experiment also clearly demonstrates that the sample volume investigated is principally confined to the region just beneath the probe surface. This point is developed further in Subsection 3.B.

B. Depth of Tissue Investigated

To quantify more precisely the volume of tissue probed in our technique, we determined the depth below the surface of each scattering event in the simulation. With this information we determined the average depth of all the scattering events for each detected photon, which we present as a probability density function in Fig. 5. To permit more general statements, distances are expressed here in mfp′ units. For typical turbid tissue[1] and near-IR wavelengths, μ_s' is around 1 mm^{-1} and μ_a is less than 0.2 mm^{-1}, which means that 1 mfp′ $\approx$ 1 mm. Figure 5 shows that the average depth of scattering is around 0.8 mfp′. Moreover it shows that for typical tissue optical properties, structures located beneath the probe at a depth greater than 2 mfp′ are not likely to contribute significantly to the measured signal (for $\rho < 1.5$ mfp′). These results are consistent with the average depth computed by Weiss *et al.*[24] using Monte Carlo simulations. However, note that their simulations do not take into account any refractive-index mismatch or a restricted numerical aperture of the detector.

To evaluate the maximum depth of photons paths, we performed experiments in Intralipid, placing the probe at the liquid surface and moving an absorbing plate placed horizontally, as described in Fig. 6. The reflectance $R(\rho, d)$ was measured for varying thickness d. The ratio $R(\rho, d)/R(\rho, d = \infty)$ is reported in Fig. 6. Figure 6 shows that the intensity of the reflectance is decreased by ~20% if the medium is 2 mfp′ thick and by ~10% if it is 3 mfp′ thick (for the albedo and the range of ρ considered). These results imply that 80% or 90% of the photons do not penetrate deeper than 2 or 3 mfp′, respectively, into the medium. This experiment complements our simulation result (Fig. 5) where the average depth of scat-

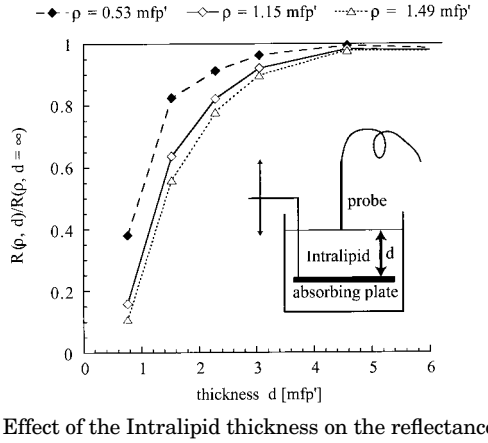

Fig. 6. Effect of the Intralipid thickness on the reflectance. The setup for the investigation of Intralipid with varying thickness is illustrated on the right-hand side. The optical coefficients of Intralipid were measured by the FDPM technique ($\lambda = 956$ nm). The reduced albedo is $a' = \mu_s'/(\mu_s' + \mu_a) = 0.98$.

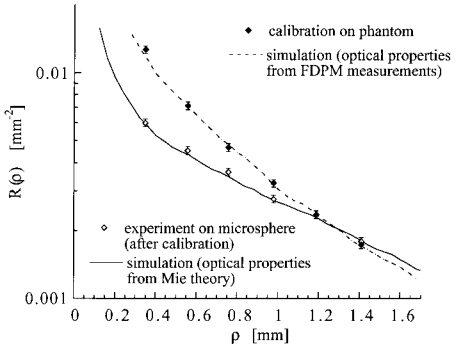

Fig. 7. Calibration measurement of a siloxane phantom and measurement test of a microsphere suspension. The siloxane phantom optical properties were measured with FDPM: $\mu_a = 0.00024 \pm 0.00002\ \text{mm}^{-1}$, $\mu_s' = 1.82 \pm 0.01\ \text{mm}^{-1}$ ($\lambda = 674$ nm). The siloxane phantom measurement is multiplied by the calibration factor to fit the corresponding simulation ($\gamma = 1.8$). The measurement on microsphere suspension is multiplied by the calibration factor derived from the siloxane phantom measurement. The simulation, corresponding to the microsphere suspension measurement, is performed by using the optical properties derived from Mie theory: $\mu_s' = 1.0\ \text{mm}^{-1}$, $\mu_a = 0.0005\ \text{mm}^{-1}$, Mie phase function ($g_1 = 0.916$, $\gamma = 2.2$).

tering was estimated to be ~1 mfp′. Thus for typical biological tissues our measurements are mainly sensitive to the region of tissue located within 2 mm of the surface and the investigated volume is of the order of 1 mm^3.

C. Calibration and Test on Microsphere Suspension

To perform absolute intensity measurements, calibration is performed on a solid turbid siloxane phantom of known μ_a and μ_s' (determined independently by FDPM).[2,3] Value $\gamma = 1.8 \pm 0.1$ was determined for the calibration phantom by consideration of the value that gives the best fit to the experimental curve, μ_a and μ_s' being fixed ($\lambda = 674$–956 nm).

As shown in Fig. 7 the phantom measurement, scaled by a single factor applied equally to all fibers, fits well the Monte Carlo simulation performed with phantom coefficients. This factor is defined as the calibration factor for a given wavelength. The calibration was performed at the end of each set of clinical measurements.

Experiments on microsphere suspensions (polystyrene sphere $\varnothing$ 1.072 ± 0.019 μm) were performed to assess the accuracy of our theoretical model and the calibration method. The scattering coefficient and the phase function of such turbid media can be known precisely by using Mie theory.[25] Because no dye was added to the suspension, μ_a was considered to be equal to the water absorption. In Fig. 7 measurement of the reflectance is compared with a simulation computed with the microsphere suspension coefficients ($\mu_s' = 1.0\ \text{mm}^{-1}$, $\mu_a = 0.00041\ \text{mm}^{-1}$, $\gamma = 2.2$). The excellent agreement found here between experiments and simulation confirms the accuracy of our simulations and the validity of our calibration procedure.

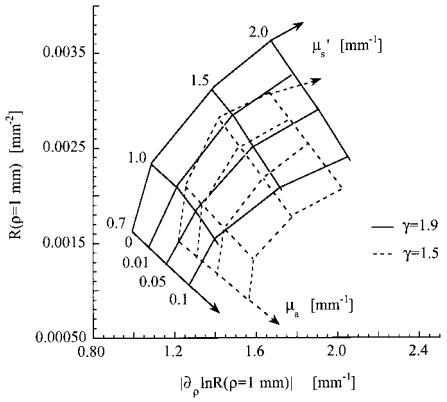

Fig. 8. Relationship between parameters $R(\rho = 1\ \text{mm})$ and $|\partial_\rho \ln R(\rho = 1\ \text{mm})|$ and the optical coefficients μ_s' and μ_a for cases of $\gamma = 1.5$ and 1.9.

D. Inverse Problem

Our goal is to solve the inverse problem that consists of extracting optical coefficients from the reflectance data. Measurements of the reflectance intensity $R(\rho)$ and the slope of ln $R(\rho)$ [denoted $\partial_\rho \ln R(\rho)$], determined at a distance $\rho = 1$ mm, can be used to derive μ_s' and μ_a for a given γ value. Figure 8 shows graphically the relationship between μ_s', and μ_a and the two parameters, $R(\rho = 1\ \text{mm})$ and $|\partial_\rho \ln R(\rho = 1\ \text{mm})|$. To illustrate the influence of parameter γ, two examples are superimposed: $\gamma = 1.5$ and $\gamma = 1.9$. We see clearly in Fig. 8 that μ_s', and μ_a cannot be determined uniquely from the two parameters, $R(\rho = 1\ \text{mm})$ and $|\partial_\rho \ln R(\rho = 1\ \text{mm})|$, if γ is unknown. This indetermination may be resolved by the values of $R(\rho)$ and/or $|\partial_\rho \ln R(\rho)|$ at other distances. Therefore the following procedure was defined for tissue measurements:

(1) Determination of μ_s' and μ_a from $R(\rho = 1\ \text{mm})$ and $|\partial_\rho \ln R(\rho = 1\ \text{mm})|$ for discrete values of γ (for example, $\gamma = 1.0, 1.5, 1.9, 2.2$).

(2) Simulations with different sets of μ_s' and μ_a obtained from Eq. (1).

(3) Comparison between the simulations and the reflectance profile for distances $0.35 < \rho < 1.4$ mm.

This last step permits us to determine the value of γ that gives the best fit. Points (1)–(3) can be done iteratively to evaluate γ more precisely. The precision that can be obtained depends on the optical coefficients themselves and on the experimental uncertainties. Nevertheless two important technical points should be noted:

First, determination of μ_s' is only weakly influenced by γ for μ_s' close to 1 mm^{-1}. Indeed in Fig. 8 the differences induced by $\gamma = 1.5$ or $\gamma = 1.9$ are typically 10% for μ_s'. In contrast, the absolute determination of μ_a is critically sensitive to γ. However, if γ remains constant, relative variations of μ_a can still be precisely evaluated. This point is discussed with the results obtained from Intralipid measurements in Subsection 3.E. Metabolism moni-

toring or drug monitoring could therefore be a potential application of such a probe.

Second, the experimental determination of $|\partial_\rho \ln R(\rho = 1\ \text{mm})|$ requires measurements at different distances close to 1 mm. To minimize errors on $|\partial_\rho \ln R(\rho = 1\ \text{mm})|$ due to experimental artifacts, we performed a fit of the reflectance curve (0.5 mm $< \rho$ 1.4 mm) with the function $m_1\rho^{m_2}\exp(-m_3\rho)$, which was always found to fit Monte Carlo simulations well for this restricted range of distances. (The same function was also proposed by Bolt and ten Bosch.[26]) Parameters $R(\rho = 1\ \text{mm})$ and $|\partial_\rho \ln R(\rho = 1\ \text{mm})|$ are then derived from the fit. Once optical coefficients μ_a and μ_s' are derived, the validity of this procedure is double-checked by comparing the curve obtained from the Monte Carlo simulation with the experimental profile.

E. Phantom Measurements

We present in this subsection measurements on tissuelike phantoms (Intralipid and microsphere suspensions). Measurements of phantoms with varying μ_a and μ_s' values were used to test the inversion procedure. For the Intralipid measurements we considered the γ value as *a priori* not known, even though γ can be estimated from published research (described below). The phantoms made of Intralipid and dye [iron(III) ferrocyanide] at different concentrations were calibrated by the FDPM technique (performed at large source–detector separations and therefore insensitive to γ). For Intralipid measurements, reflectance profiles were found to fit best when the parameter γ was between 1.6 and 1.8 for $\lambda = 674-849$ nm. The μ_a values derived from our method are plotted in Fig. 9(a) versus the values obtained by the FDPM technique. Figure 9(a) shows that $\gamma = 1.8$ leads to an overestimation of μ_a by $\sim 0.005\ \text{mm}^{-1}$, whereas $\gamma = 1.6$ leads to an underestimation of μ_a by $\sim 0.01\ \text{mm}^{-1}$. This example clearly illustrates that determination of the absolute values of μ_a are sensitive to γ. However, changes in the absorption coefficient can be measured to within $\pm 0.005\ \text{mm}^{-1}$.

The accuracy of the inversion procedure on μ_s' is illustrated in Fig. 9(b). In the case of μ_s', as mentioned above, the influence of γ is weaker than in the case of μ_a. A difference of only 5% is found on the μ_s' if $\gamma = 1.6$ is used instead of 1.8. This is also approximately the variation in μ_s' values obtained by multiple FDPM measurements. We also found that in the case of a constant Intralipid concentration the measured values of μ_s' vary by less than 2% when μ_a is increased from 0.012 to $0.5\ \text{mm}^{-1}$ by the addition of dye, which proves that the data-inversion procedure effectively uncouples μ_a and μ_s'.

From our measurements, γ can be estimated to $\gamma = 1.7 \pm 0.1$ ($\lambda = 675$ nm). The calculation when Mie theory was used and the size distribution given by van Staveren *et al.*[27] leads to $\gamma = 1.89$ ($\lambda = 675$ nm). These values are in good agreement considering that the actual size distribution of the sample may slightly vary from the sample measured by van Staveren *et al.* Note also that they found a similar discrepancy for g_1 between Mie theory and experiments.

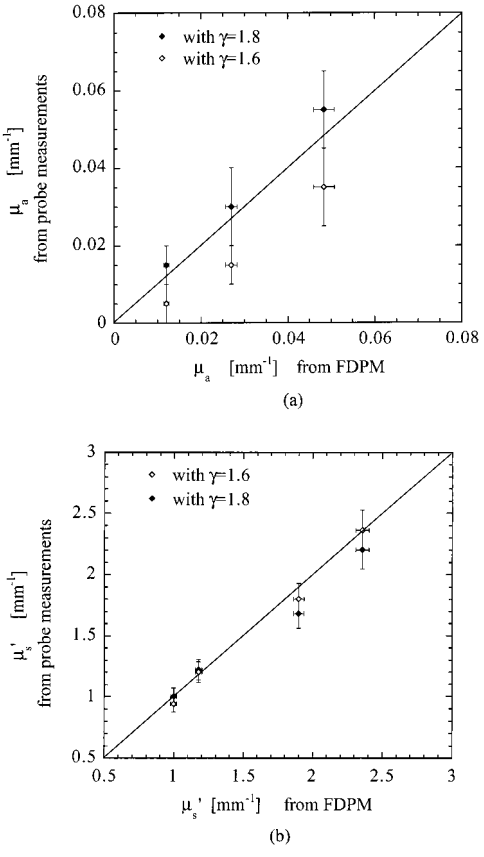

Fig. 9. Comparison between (a) μ_a, and (b) μ_s' obtained by the FDPM technique and by probe measurements. Measurements are on Intralipid [(a) with dye; (b) without dye].

Further assessments of the inversion procedure were performed on monodisperse microsphere suspensions. In this case we considered the γ value as *a priori* known from Mie theory: $\gamma = 2.2$ (polystyrene, $\varnothing = 1.053 \pm 0.010$ μm, $\lambda = 675$ nm). The optical coefficients derived from our local reflectance measurements are compared with values obtained with a spatially resolved transmittance method described elsewhere.[22,23]

Figures 10(a) and 10(b) show μ_a and μ_s' values obtained by both methods: spatially resolved transmittance and reflectance. Phantoms made of microsphere suspensions and ink at different concentrations were used. An excellent correlation is found between the μ_a and μ_s' values obtained by the two methods. Small systematic differences (typically 10%) are found when comparing absolute values. They are mainly due to errors occurring in the calibration procedures (for both methods). A further comparison with Mie theory also showed a typical deviation of 2% for μ_s' (a maximum deviation of 10%). The relatively small errors that we found here are typical of errors found when different techniques for measuring turbid-media optical properties are compared.[28] Such errors could be avoided by multiple calibrations on several turbid samples of different

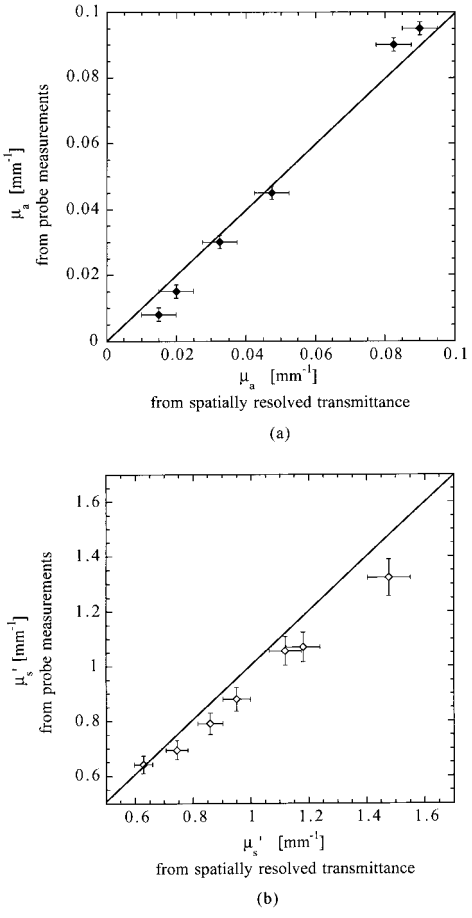

Fig. 10. Comparison between (a) μ_a, and (b) μ_s', obtained from spatially resolved transmittance (the method described in Refs. 22 and 23) and from probe measurements. Measurements are on microsphere suspensions [(a) with ink; (b) without ink].

known optical properties. However, the accuracy of tissue measurements is subject to other major limitations due to, for example, their structure and heterogeneity.[29] Therefore more accurate calibration is not necessarily required for absolute tissue measurements, since we are mainly interested in observing optical-property differences between tissue physiological states.

F. *In vivo* Measurements on Brain Tissues

Clinical measurements of normal and malignant neural tissues were recorded *in vivo* during brain surgery.[30] Two different cases are reported here. Case 1 was a 3-year-old male and case 2 was an 8-year-old male. Different types of tissues were investigated in each case. Several measurements (typically six) were always performed successively at a given location. The intensity fluctuations (typically of the order of 10%) for these measurements were mainly due to tissue heterogeneity and slight probe movements. The average reflectance was calculated for each location as well as the standard deviation. Note that the uncertainty due to the apparatus, estimated from measurements on a phantom, is much lower (<5%). Before each set of measurements the blood from the surgical site was carefully irrigated away with saline and the probe was cleaned with a saline-damped sponge. The measurements presented here were performed in parallel with frequency-domain measurements[2,3] (FDPM) by using a source–detector separation of 10–14 mm.

In case 1 measurements were performed on normal cerebral cortex (frontal lobe and temporal lobe), optic nerve astrocytoma (size, ≈1.3 cm), and normal optic nerve. In case 2 measurements were performed on the skull, deep cerebellar white matter with scar tissue (from a previous surgery), medulloblastoma (size, ≈3.8 cm), and deep cerebellar white matter. Tumor dimensions were estimated from conventional imaging techniques (i.e., computed tomography and/or magnetic resonance imaging).

As discussed in Subsection 3.B, the depth probed is less than ~2 mm. For each type of tissue that we investigated the influence of surrounding tissues on the measurement is weak. In particular, only gray matter is investigated during measurements of the cerebral cortical surface.

Figures 11(a) and 11(b) show the measured parameters $R(\rho = 1\ \text{mm})$ as a function of $|\partial \ln R(\rho = 1\ \text{mm})|$ obtained for cases 1 and 2, respectively. They are similar to Fig. 8 except that the relationship between parameters $R(\rho = 1\ \text{mm})$ and $|\partial_\rho \ln R(\rho = 1\ \text{mm})|$ and optical coefficients μ_a and μ_s' is indicated only qualitatively by two arrows for better clarity. (Different grids corresponding to different γ values should be superimposed.) Quantitative results are reported in Tables 1 and 2.

Figures 11(a) and 11(b) show that parameters $R(\rho = 1\ \text{mm})$ and $|\partial_\rho \ln R(\rho = 1\ \text{mm})|$ provide excellent discrimination between tissue types. The spectroscopic signature on $R(\rho = 1\ \text{mm})$ and $|\partial_\rho \ln R(\rho = 1\ \text{mm})|$ should also be noted. The cortex and the skull exhibit less significant spectroscopic differences compared with tumor tissues such as the astrocytoma and the medulloblastoma. Thus parameters $R(\rho = 1\ \text{mm})$ and $|\partial_\rho \ln R(\rho = 1\ \text{mm})|$ could be useful for optical biopsy. Nevertheless we believe that to exploit these results fully the differences found must be explained in terms of scattering and absorption parameters. These factors in turn can be used to understand physiological and structural variations. The procedure described in Subsection 3.D was used to determine coefficients μ_s', μ_a, and γ from the measured curves. This procedure is fully illustrated for measurements of the temporal lobe. Results of optical coefficient calculations are summarized for all tissues in Tables 1 and 2. Values obtained in parallel by the FDPM technique are also indicated.

Figure 12 shows that the best fit to the cortex (temporal lobe) data is obtained with $\gamma = 1.9$. Lower values, such as $\gamma = 1.5$, led to impossible values for $R(\rho = 1\ \text{mm})$ and $|\partial_\rho \ln R(\rho = 1\ \text{mm})|$ and should therefore be rejected. Larger values, such as $\gamma = 2.2$, do not fit the reflectance data for distances $\rho < 0.8$ mm. The γ value is then estimated to be $\gamma = 1.9 \pm 0.2$. Note that $\gamma = 2.2$ would lead

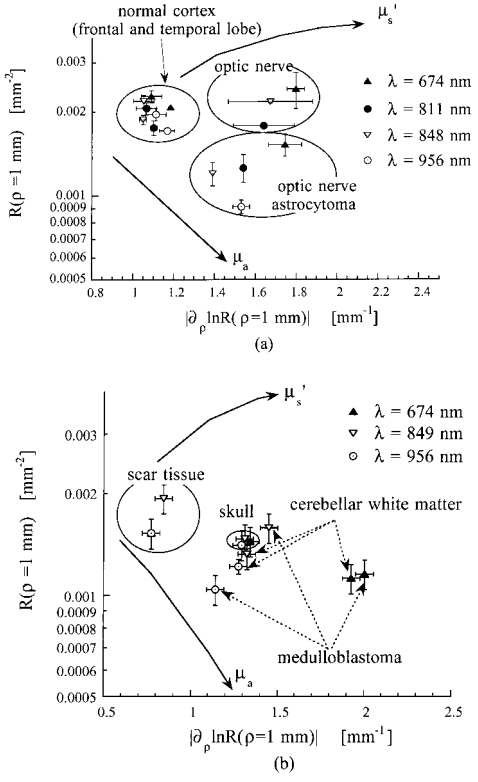

Fig. 11. Clinical measurements *in vivo* on human brain for (a) case 1 and (b) case 2. Plot of $R(\rho = 1)$ and $|\partial_\rho \ln R(\rho = 1\ \text{mm})|$ for different types of brain tissue: (a) normal cortex (frontal and temporal lobe), optic nerve astrocytoma, and normal optic nerve; (b) skull, deep cerebellar white matter with scar tissue, medulloblastoma, and deep cerebellar white matter (surrounding normal tissue).

to almost identical μ_s' (differences of less than 5%) and an overestimation of μ_a of $\sim 0.02\ \text{mm}^{-1}$. Taking into account the uncertainties of the measurements [$\sim$5% on $R(\rho = 1\ \text{mm})$ and $|\partial_\rho \ln R(\rho = 1\ \text{mm})|$ for this tissue] and the uncertainty of γ (± 0.2), the error of the absolute value of μ_s' is estimated to be 5%.

In some cases, as shown, for example, in Fig. 12, the nearest fiber does not perfectly fit the simulation. Different reasons may be suggested. First, this fiber is at the limit of the region where only the parameter γ must be taken into account. Therefore higher moments of the phase function may also be considered. Second, this fiber probes the tissue more superficially than the other fibers (see Fig. 5), and the differences that occur at the nearest fiber may be due also to tissue heterogeneity.

As reported in Table 1, with the exception of the normal optic nerve, the absorption coefficients at 811 and 849 nm are lower than those obtained at $\lambda = 674$ nm or $\lambda = 956$ nm. This result is consistent with the fact that the main near-IR tissue chromophores, hemoglobin and water, have an absorption maximum at approximately $\lambda < 700$ nm and $\lambda = 970$ nm, respectively.[31] The overall absorption is much higher in the tumor than the cortex presumably because of the greater hemoglobin in the tumor. Tumors generally grow more new blood vessels and thus have a higher hemoglobin concentration.

The μ_s' of the tumor is similar to the cortex at $\lambda = 956$ nm. However, the variation of μ_s' between $\lambda = 674$ nm and $\lambda = 956$ nm is much larger for the tumor than for the cortex: $\Delta\mu_s' \approx 0.57\ \text{mm}^{-1}$ for tumor and $\Delta\mu_s' \approx 0.10\ \text{mm}^{-1}$ for the cortex. Such spectroscopic variations may be attributable to structural differences between tissue types. Indeed such differences may depend on the average size or size distribution of scattering structures within or between cells.

Higher scattering is found for the normal optic nerve compared with all the other tissues in case 1. This is likely due to the presence of myelin. *In vitro* measurements have also shown that myelin containing white matter exhibits a higher scattering coeffi-

Table 1. Optical Properties of Normal and Malignant Human Brain Tissue, Case 1

Type of Tissue	Wavelength (nm)	Probe Measurements			FDPM[a]	
		γ	μ_s' (mm^{-1})	μ_a (mm^{-1})	μ_s' (mm^{-1})	μ_a (mm^{-1})
Cortex (frontal lobe)	674	1.9 ± 0.2	1.00 ± 0.05	<0.02 ± 0.01	1.12	0.0173
	811	1.9 ± 0.2	0.91 ± 0.05	<0.01 ± 0.01	0.74	0.0182
	849	1.9 ± 0.2	0.92 ± 0.05	<0.01 ± 0.01	0.74	0.0185
	956	1.9 ± 0.2	0.89 ± 0.05	0.015 ± 0.01	0.80	0.0206
Cortex (temporal lobe)	674	1.9 ± 0.2	1.00 ± 0.05	0.02 ± 0.01	0.99	0.0179
	811	1.9 ± 0.2	0.82 ± 0.05	0.02 ± 0.01	0.48	0.0190
	849	1.9 ± 0.2	0.82 ± 0.05	<0.01 ± 0.01	0.45	0.0179
	956	1.9 ± 0.2	0.82 ± 0.05	0.025 ± 0.01	0.42	0.0218
Astrocytoma of optic nerve	674	1.7 ± 0.2	1.25 ± 0.10	0.14 ± 0.03	0.92	0.0165
	811	1.7 ± 0.2	0.95 ± 0.10	0.12 ± 0.03	0.55	0.0190
	849	1.7 ± 0.2	0.76 ± 0.10	0.09 ± 0.03	0.59	0.0191
	956	1.7 ± 0.2	0.73 ± 0.10	0.15 ± 0.03	0.58	0.0323
Normal optic nerve	674	1.7 ± 0.2	1.75 ± 0.20	0.06 ± 0.03	N/A	N/A
	811	1.7 ± 0.2	N/A	N/A	N/A	N/A
	849	1.7 ± 0.2	1.60 ± 0.20	0.08 ± 0.03	N/A	N/A
	956	1.7 ± 0.2	1.52 ± 0.20	0.07 ± 0.03	N/A	N/A

[a]The uncertainty of the FDPM values, given by the fitting procedure (see Refs. 2 and 3), is typically 2%.

Table 2. Optical Properties of Normal and Malignant Human Brain Tissue, Case 2

Type of Tissues	Wavelength (nm)	Probe Measurements			FDPM*	
		γ	μ_s' (mm^{-1})	μ_a (mm^{-1})	μ_s' (mm^{-1})	μ_a (mm^{-1})
Skull	674	1.9 ± 0.2	0.9 ± 0.1	0.05 ± 0.02	1.19	0.0208
	849	1.9 ± 0.2	0.9 ± 0.1	0.05 ± 0.02	0.91	0.0215
	956	1.9 ± 0.2	0.85 ± 0.1	0.05 ± 0.02	0.77	0.0355
Cerebellar white matter	674	1.9 ± 0.2	1.35 ± 0.1	0.25 ± 0.05	1.34	0.0165
	849	1.9 ± 0.2	0.85 ± 0.1	0.095 ± 0.02	0.98	0.0132
	956	1.9 ± 0.2	0.78 ± 0.1	0.090 ± 0.02	0.84	0.0299
Medulloblastoma	674	1.9 ± 0.2	1.40 ± 0.1	0.26 ± 0.05	1.05	0.0120
	849	1.9 ± 0.2	1.07 ± 0.1	0.10 ± 0.02	0.66	0.0079
	956	1.9 ± 0.2	0.4 ± 0.1	0.075 ± 0.02	0.54	0.0239
Cerebellar white matter with scar tissues	674	2.2 ± 0.2	0.65 ± 0.05	<0.02	N/A	N/A
	849	2.2 ± 0.2	0.80 ± 0.05	<0.02	N/A	N/A
	956	2.2 ± 0.2	0.65 ± 0.05	<0.02	N/A	N/A

[a]The uncertainty of the FDPM values, given by the fitting procedure (see Refs. 2 and 3), is typically 2.5%.

cient compared with other tissue.[12,19,23] The accuracy of the measurement on the optic nerve tissue can be affected by the high anisotropy of this type of tissue. Indeed it has been reported that light propagation depends on whether the direction considered is parallel or perpendicular to the nerve fibers.[32–34] Interestingly, comparison between measurements with the two symmetric sources reveals larger differences than for the other tissues. This variation is represented in Fig. 11(a) by the relatively large uncertainties associated with the optic nerve measurements.

In case 2 the first measurements were acquired directly from the skull. The difference in reduced scattering properties between $\lambda = 674$ and 956 nm is very small ($\mu_s' = 0.9$ and 0.85 mm^{-1}, respectively) as shown in Fig. 11(b). Previously determined *in vitro* values[35] for pig skull were approximately twice as large. Such differences may be due to variations in water content and sample preparation between *in vivo* and *in vitro* studies.

Case 2 data were also obtained from in series deep cerebellar white matter with scar tissue, tumor (medulloblastoma), and cerebellar white matter in the excavated tumor bed. Figure 11(b) shows that scar tissue is well differentiated from other structures and is characterized by a high γ value ($\gamma = 2.2$) and low absorption ($\mu_a < 0.02$ mm^{-1}), which is consistent with the low vascularization of such tissue. In contrast, larger μ_a, smaller γ, and large spectroscopic differences in μ_s' are found in white matter and medulloblastoma. As in case 1 the large μ_a values obtained for the tumor can be related to higher hemoglobin content, as is often found for cancerous tissues. Taking into account measurement variability, no significant differences are found between the tumor and the surrounding normal white matter. However, it is not clear that the so-called normal tissue measured at the surgical boarder could be considered disease-free and unaffected by the tumor vasculature.

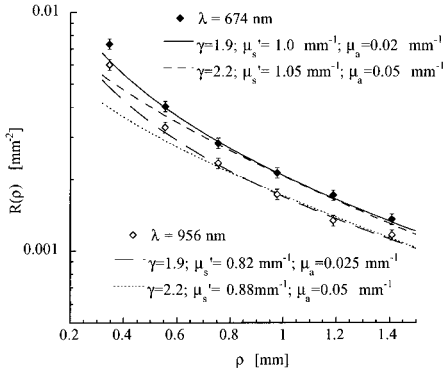

Fig. 12. Comparison between the spatially resolved reflectance curve measured *in vivo* on normal cortex (temporal lobe) and simulations.

Some of the different types of tissue examined here showed a dependence on the phase-function parameter γ. This confirms that γ may be a valuable parameter for tissue characterization. Nevertheless an improvement in the accuracy of the γ determination would be necessary to conclude the importance of this parameter.

The optical coefficients that we obtained can be compared with measurements performed simultaneously with the FDPM technique. One should keep in mind that the depth investigated by the FDPM technique is greater compared with the spatially resolved technique described here. Generally the μ_s' values are similar between the two methods, whereas more differences are found for μ_a. For the cortex and the skull measurements both μ_s' and μ_a values are generally in good agreement. The decrease in μ_s' from $\lambda = 674$–956 nm is more pronounced in the FDPM data. In contrast, important differences are found for μ_a results where tumor values (astrocytoma and medulloblastoma) obtained by FDPM are significantly lower. This can be explained by the sensitivity of the spatially resolved probe to the high local hemoglobin content that can be resolved only by the small source–detector separations. In contrast the large source–detector sep-

aration employed by the FDPM probe interrogates much greater larger-tissue volumes and hence measures average optical properties from multiple structures (e.g., normal + malignant).

4. Conclusions

The purpose of this research was to assess the performance of spatially resolved reflectance by using short source–detector separations (<1.4 mm). Monte Carlo simulations, the accuracy of which were confirmed by experiments on tissue phantoms, were used to establish the correspondence between the measured reflectance and the optical properties.

Optical properties that can be determined by this technique are the absorption coefficient μ_a, the reduced scattering coefficient μ_s', and a parameter of the phase function $\gamma = (1 - g_2)/(1 - g_1)$, where $g_1(=g)$ and g_2 are the first and the second moment of the phase function. Experiments on calibrated Intralipid solutions and microsphere suspensions showed that changes in the absorption coefficient, reduced scattering coefficient, and γ can be measured to within $\pm 0.005\ \mathrm{mm}^{-1}$, $\pm 0.05\ \mathrm{mm}^{-1}$, and ± 0.2 respectively. Systematic errors are possible if the parameter γ is not determined with sufficient accuracy. These performances could be improved by lowering the uncertainty on reflectance measurements.

Experiments and simulations helped to define the average volume probed by this technique. For typical tissues the average probe depth is typically ~1 mm and the influence of layers located below 3 mm is negligible.

Finally *in vivo* measurements on human brain showed that excellent discrimination can be obtained between different types of neural tissues, normal and abnormal. Good correlation has been found between spatially resolved reflectance and simultaneous measurements performed by FDPM. These two techniques offer interesting complementary features. The spatially resolved probe can potentially provide better differentiation between different types of tissue owing to its sensitivity to local structure, because substantially a smaller volume of tissue is probed. On the other hand, owing to physical limitations imposed by large near-IR mean absorption lengths in tissue, the precision for the μ_a estimate is likely to be worse. Consequently, the short distance, spatially resolved technique appears to be well suited for clinical settings that require rapid localized tissue identification, such as endoscopic or a needle-based optical biopsy, and intraoperative tissue mapping for surgical guidance.

We are grateful to O. Coquoz, J. B. Fishkin, T. H. Pham, V. Venugopalan, and D. Jakubowski for help with the FDPM measurements and data processing. We also thank P. Fankhauser for help with designing the probe. We acknowledge the Department of Microengineering, Swiss Federal Institute of Technology-Lausanne for the Visiting Faculty Fellowship Program. This research was supported by the Swiss National Science Foundation [(2053-049628.96) National Institutes of Health (NIH) Laser Microbeam and Medical Program (LAMMP) and Optical Biology facilities (grants RR-01192 and CA-62203, respectively)], NIH grant GM-50958, and Department of Energy grant DE-FG03-91ER61227.

References and Notes

1. W.-F. Cheong, S. A. Prahl, and A. J. Welch, "A review of the optical properties of biological tissues," IEEE J. Quantum Electron. **26,** 2166–2185 (1990).
2. J. B. Fishkin, O. Coquoz, E. R. Anderson, M. Brenner, and B. J. Tromberg, "Frequency-domain photon migration measurements of normal and malignant tissue optical properties in a human subject," Appl. Opt. **36,** 10–20 (1997).
3. B. J. Tromberg, O. Coquoz, J. B. Fishkin, T. Pham, E. R. Anderson, J. Butler, M. Cahn, J. D. Gross, V. Venugopalan, and D. Pham, "Noninvasive measurements of breast tissue optical properties using frequency-domain photon migration," Philos. Trans. R. Soc. London Ser. B **352,** 661–668 (1997).
4. J. R. Mourant, I. J. Bigio, J. Boyer, R. L. Conn, T. Johnson, and T. Shimada, "Spectroscopic diagnosis of bladder cancer with elastic light scattering," Lasers Surg. Med. **17,** 350–357 (1995).
5. T. J. Farrell, M. S. Patterson, and B. C. Wilson, "A diffusion theory model of spatially resolved, steady-state diffuse reflectance for the noninvasive determination of tissue optical properties *in vivo*," Med. Phys. **19,** 879–888 (1992).
6. R. Bays, G. Wagnières, D. Robert, D. Braichotte, J.-F. Savary, P. Monnier, and H. van den Bergh, "Clinical determination of tissue optical properties by endoscopic spatially resolved reflectometry," Appl. Opt. **35,** 1756–1766 (1996).
7. A. Kienle, L. Lilge, M. S. Patterson, R. Hibst, R. Steiner, and B. C. Wilson, "Spatially resolved absolute diffuse reflectance measurements for noninvasive determination of the optical scattering and absorption coefficients of biological tissue," Appl. Opt. **35,** 2304–2314 (1996).
8. S. Fantini, M. A. Franceschini, J. B. Fishkin, B. Barbieri, and E. Gratton, "Quantitative determination of the absorption spectra of chromophores in strongly scattering media: a light-emitting-diode based technique," Appl. Opt. **33,** 5204–5213 (1994).
9. G. Mitic, J. Kölzer, J. Otto, E. Plies, G. Sölkner, and W. Zinth, "Time-gated transillumination of biological tissues and tissue-like phantoms," Appl. Opt. **33,** 6699–6710 (1994).
10. G. Kumar and J. M. Schmitt, "Optimal probe geometry for near-infrared spectroscopy of biological tissue," Appl. Opt. **36,** 2286–2293 (1997).
11. J. R. Mourant, I. J. Bigio, D. A. Jack, T. M. Johnson, and H. D. Miller, "Measuring absorption coefficients in small volumes of highly scattering media: source-detector separations for which path lengths do not depend on scattering properties," Appl. Opt. **36,** 5655–5661 (1997).
12. F. Bevilacqua, "Optical characterization of biological tissues *in vitro* and *in vivo*," Ph.D. dissertation 1781 (Swiss Federal Institute of Technology, Lausanne, 1998).
13. F. Bevilacqua and C. Depeursinge, "Monte Carlo study of diffuse reflectance at source–detector separations close to one transport mean free path," submitted to J. Opt. Soc. Am. A.
14. F. P. Bolin, L. E. Preuss, R. C. Taylor, and R. J. Ference, "Refractive index of some mammalian tissues using a fiber optic cladding method," Appl. Opt. **28,** 2297–2303 (1989).
15. D. R. Wyman, M. S. Patterson, and B. C. Wilson, "Similarity relations for anisotropic scattering in Monte Carlo simulations of deeply penetrating neutral particles," J. Comput. Phys. **81,** 137–150 (1989).
16. H. C. van de Hulst, *Multiple Light Scattering, Tables, Formulas, and Applications* (Academic, London, 1980).
17. S. L. Jacques, C. A. Alter, and S. A. Prahl, "Angular depen-

dance of HeNe laser light scattering by human dermis," Lasers Life Sci. **1,** 309–333 (1987).
18. R. Marchesini, A. Bertoni, S. Andreola, E. Melloni, and A. E. Sichirollo, "Extinction and absorption coefficients and scattering phase functions of human tissues *in vitro*," Appl. Opt. **28,** 2318–2324 (1989).
19. P. van der Zee, M. Essenpreis, and D. T. Delpy, "Optical properties of brain tissue," in *Photon Migration and Imaging in Random Media and Tissues*, B. Chance and R. R. Alfano, eds., Proc. SPIE **1888,** 454–465 (1993).
20. S. T. Flock, B. C. Wilson, and M. S. Patterson, "Total attenuation coefficient and scattering phase functions of tissues and phantom materials at 633 nm," Med. Phys. **14,** 835–841 (1987).
21. R. Graaff, A. C. M. Dassel, M. H. Koelink, F. F. M. de Mul, J. G. Aarnoudse, and W. G. Zijlstra, "Optical properties of human dermis *in vitro* and *in vivo*," Appl. Opt. **32,** 435–447 (1993).
22. P. Marquet, F. Bevilacqua, C. Depeursinge, and E. B. de Haller, "Determination of reduced scattering and absorption coefficients by a single charge-coupled-device array measurement, part I: comparison between experiments and simulations," Opt. Eng. **34,** 2055–2063 (1995).
23. F. Bevilacqua, P. Marquet, C. Depeursinge, and E. B. de Haller, "Determination of reduced scattering and absorption coefficients by a single charge-coupled-device array measurement, part II: measurements on biological tissues," Opt. Eng. **34,** 2064–2069 (1995).
24. G. H. Weiss, R. Nossal, and R. F. Bonner, "Statistics of penetration depth of photons reemitted from irradiated tissue," J. Mod. Opt. **36,** 349–359 (1989).
25. C. F. Bohren and D. R. Huffman, *Absorption and Scattering of Light by Small Particles* (Wiley, New York, 1983).
26. J. R. A. Bolt and J. J. ten Bosch, "Method for measuring position-dependent volume reflection," Appl. Opt. **32,** 4641–4645 (1993).
27. H. J. van Staveren, C. J. M. Moes, J. van Marle, S. A. Prahl, and Martin J. C. van Gemert, "Light scattering in Intralipid-10% in the wavelength range of 400–1100 nm," Appl. Opt. **30,** 4507–4514 (1991).
28. S. J. Madsen, B. C. Wilson, M. S. Patterson, Y. D. Park, S. L. Jacques, and Y. Hefetz, "Experimental tests of a simple diffusion model for the estimation of scattering and absorption coefficients of turbid media from time-resolved diffuse reflectance measurements," Appl. Opt. **31,** 3509–3517 (1992).
29. F. Bevilacqua, P. Marquet, O. Coquoz, and C. Depeursinge, "Role of tissue structure in photon migration through breast tissues," Appl. Opt. **36,** 44–51 (1997).
30. Protocol and informed consent were obtained from the patient undergoing neurological surgery for an intra-axial brain tumor as demonstrated on conventional neuroimaging. The protocol and informed consent documents were approved by the University of California Irvine review board (HS 96-495).
31. M Cope, "The development of a near infrared spectroscopy system and its application for noninvasive monitoring of cerebral blood and tissue oxygenation in the newborn infant," Ph.D. dissertation (University College London, London, 1991).
32. K. M. Hebeda, T. Menovsky, J. F. Beek, J. G. Wolbers, and M. J. C. van Gemert, "Light propagation in the brain depends on nerve fiber orientation," Neurosurgery, **35,** 720–722 (1994).
33. D. R. Sandeman, T. Mills, and S. G. Bown, "Enhancement of light penetration by white matter tracts in the normal mouse brain," Lasers Med. Sci. **3,** 47 (1986).
34. J. G. Wolbers, W. Kamphorst, H. J. M. Sterenborg, M. J. C. van Gemert, and W. Hogervorst, "Dose response of rat brains interstitially irradiated by argon light," Lasers Med. Sci. **2,** 255–260 (1987).
35. M. Firbank, M. Hiraoka, M. Essenpreis, and D. T. Delpy, "Measurements of the optical properties of the skull in the wavelength range 650–950 nm," Phy. Med. Biol. **38,** 503–510 (1993).